Available online at www.sciencedirect.com

ScienceDirect

International Journal of Solids and Structures 45 (2008) 1954–1977

INTERNATIONAL JOURNAL OF SOLIDS AND STRUCTURES

www.elsevier.com/locate/ijsolstr

An asymptotic analysis of composite beams with kinematically corrected end effects

Jun-Sik Kim [a,*], Maenghyo Cho [b], Edward C. Smith [a]

[a] *The Pennsylvania State University, University Park, PA 16802, USA*
[b] *Seoul National University, Seoul 151-742, Republic of Korea*

Received 11 July 2007; received in revised form 2 November 2007
Available online 19 November 2007

Abstract

A finite element-based beam analysis for anisotropic beams with arbitrary-shaped cross-sections is developed with the aid of a formal asymptotic expansion method. From the equilibrium equations of the linear three-dimensional (3D) elasticity, a set of the microscopic 2D and macroscopic 1D equations are systematically derived by introducing the virtual work concept. Displacements at each order are split into two parts, such as fundamental and warping solutions. First we seek the warping solutions via the microscopic 2D cross-sectional analyses that will be smeared into the macroscopic 1D beam equations. The variations of fundamental solutions enable us to formulate the macroscopic 1D beam problems. By introducing the orthogonality of asymptotic displacements to six beam fundamental solutions, the end effects of a clamped boundary are kinematically corrected without applying the sophisticated decay analysis method. The boundary conditions obtained herein are applied to composite beams with solid and thin-walled cross-sections in order to demonstrate the efficiency and accuracy of the formal asymptotic method-based beam analysis (FAMBA) presented in this paper. The numerical results are compared to those reported in literature as well as 3D FEM solutions.

Keywords: Composite beam; Formal asymptotic method; End effects; Boundary condition; Cross-sectional analysis

1. Introduction

Slender beam structures made of composite materials have found many useful applications in aerospace engineering, civil engineering and the automobile industry. One of the active research fields is the modelling of composite rotor blades used on helicopters and tiltrotor aircrafts (Hodges, 1990; Jung et al., 1999; Volovoi et al., 2001). In general, one may successfully apply a classical beam theory (i.e., the beam deformation is defined by the classical strain measure associated with extension, bending, and torsion) if the beam is sufficiently slender, i.e., $\epsilon \to 0$ (ϵ is the ratio of the maximum dimension of a beam cross-section to the characteristic length of the beam). It is, however, not adequate for an analysis of the beam made of a strongly

* Corresponding author. Tel.: +1 814 865 1986.
E-mail address: jskim@psu.edu (J.-S. Kim).

0020-7683/$ - see front matter
doi:10.1016/j.ijsolstr.2007.11.005

anisotropic composite, especially one weak in shear. Thus refined beam theories have been developed to improve the prediction of behavior of composite beams. It has been, however, turned out to be unnecessary to develop refined beam theories for composite box beams studied extensively in literature (Volovoi et al., 2001), since the slenderness of composite box beams selected is within the validity of a classical beam theory. In spite of that, several refined theories have failed to accurately predict the elastostatic behavior of such beams. This is quite different from plate and shell theories. Indeed, unlike plate and shell structures in which Poisson's effect is dominant in the reduced dimension (i.e., thickness), the thin-walled structure exhibits more complex deformations on the cross-section such as bending deformation and distortion of thin-walls.

Although a classical beam theory is adequate for many engineering applications (Trabucho and Viãno, 1996), one may need to obtain high accuracy for other applications such as high frequency vibrations, sandwich beams and thin-walled open-section beams. In general, a Rankine–Timoshenko-type beam theory is required for most engineering applications. The Vlasov theory is, however, more important than the Rankine–Timoshenko one when the considered beam falls into the category of thin-walled open-section beams. A treatment of torsional warping restrained effect belongs to the boundary layer problems in the asymptotic sense (Balch and Steele, 1987). As far as the interior solutions are concerned, considering such an effect may need a special treatment. For instance, one can promote the order of magnitude of the warping function related to the cross-sectional distortion mode (Yu et al., 2005). In this paper, we shall focus on Rankine–Timoshenko corrections to elementary (or classical) beam theory by using a formal asymptotic expansion method.

An asymptotic method is a mathematically rigorous means to analyze beam structures. There are two types of asymptotic methods at least; one is a formal asymptotic expansion method (FAM) (Trabucho and Viãno, 1996) and the other is a variational-asymptotic method (VAM) pioneered by Berdichevsky (1981). It is, however, troublesome in both methods to obtain the higher-order effects, such as transverse shear deformations, in the 1D beam response because it requires a proper set of boundary conditions. In order to circumvent this, Hodges and his co-workers (Cesnik et al., 1996; Popescu and Hodges, 2000; Yu et al., 2002) have devoted to deriving a Rankine–Timoshenko-like beam theory based on the finite element cross-sectional analysis by applying the VAM. The most recent version of such efforts has been made by Yu et al. (2002) via the so-called Timoshenko-like energy transformation. These have been referred to as variational-asymptotic beam sectional analysis (VABS) since the work of Cesnik and Hodges (1997).

On the other hand, there have been several efforts (Duva and Simmonds, 1991; Fan and Widera, 1992; Buannic and Cartraud, 2000; Buannic and Cartraud, 2001b) to obtain the exact interior solution using a formal asymptotic method by finding asymptotically correct boundary conditions with the aid of a decay analysis method developed by Gregory and Wan (1984). It is, however, too difficult to find these boundary conditions by applying a decay method for engineering applications. One can avoid such difficulty by obtaining simplified boundary conditions while providing reasonable accuracy (i.e., Rankine–Timoshenko corrections to elementary beam theory). Such boundary conditions were derived by Horgan and Simmonds (1991) and applied to orthotropic beams weak in shear (Duva and Simmonds, 1992). In Section 5, these simplified boundary conditions will be discussed in detail.

In this paper, we follow and generalize the way described in Buannic and Cartraud (2000, 2001a) via the virtual work concept as well as finite element method. A formal asymptotic method-based beam analysis (FAMBA) is developed to analyze anisotropic beams with arbitrary cross-sections, which is completely realized with 2D four-noded and 1D three-noded finite elements for microscopic and macroscopic problems, respectively. Simplified boundary conditions mentioned in the above are generalized by introducing an orthogonality of asymptotic displacements to six beam fundamental displacements as constraint equations. In this way, a set of recursive beam equations along with proper boundary conditions are obtained in the weak form, which yields comparable results to the Rankine–Timoshenko theory. The results obtained herein are asymptotically correct up to $O(\epsilon^2)$ and are compared to those available in literature and 3D FEM solutions for a sandwich beam with solid cross-section and thin-walled composite box beams.

2. Formal asymptotic expansion method

A 3D slender beam is considered in this study, which has arbitrary cross-section geometry and material anisotropy (Fig. 1). In order to apply the asymptotic expansion method by taking the advantage of slenderness

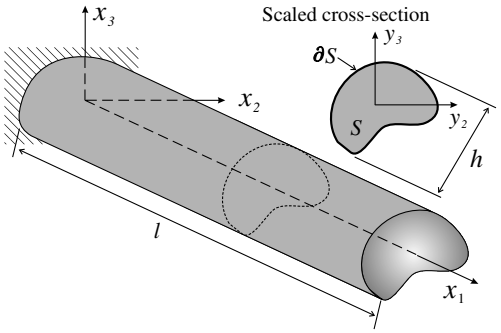

Fig. 1. A 3D slender composite structure.

of beam structures, one needs to define the small parameter, ϵ, first. To this end, the beam cross-section is scaled in the following manner:

$$y_1 = x_1, \quad y_2 = \frac{x_2}{\epsilon}, \quad y_3 = \frac{x_3}{\epsilon}, \tag{1}$$

in which a small parameter, ϵ, is defined as

$$\epsilon = \frac{h}{l_c}, \tag{2}$$

where h and l_c represent the maximum dimension of the beam cross-section and the characteristic length of the beam, respectively.

The axial coordinate, x_1, is chosen to be passing through the centroid of cross-sections (Trabucho and Viãno, 1996). It has the following properties

$$\langle x_2 \rangle = \langle x_3 \rangle = \langle x_2 x_3 \rangle = 0, \tag{3}$$

where $\langle \bullet \rangle = \int_S \bullet \, \mathrm{d}S$.

2.1. 3D formulation and asymptotic expansions

By employing the scaled coordinates presented in Eq. (1), the 3D static problem of a linear elasticity, which consists of equilibrium equations, strain–displacement relationships and constitutive equations, can be expressed as follows:

$$\begin{aligned}
&\sigma_{ij,j} + \tilde{b}_i = 0 \rightarrow \frac{1}{\epsilon}\mathcal{L}_{23}^t \sigma + \mathcal{L}_1^t \sigma_{,1} + \tilde{\mathbf{b}} = 0, \\
&\varepsilon_{ij} = \frac{1}{2}(u_{i,j} + u_{j,i}) \rightarrow \varepsilon = \frac{1}{\epsilon}\mathcal{L}_{23}\mathbf{u} + \mathcal{L}_1 \mathbf{u}_{,1}, \\
&\sigma_{ij} = c_{ijkl}\varepsilon_{kl} \rightarrow \sigma = \frac{1}{\epsilon}\mathbf{C}\mathcal{L}_{23}\mathbf{u} + \mathbf{C}\mathcal{L}_1 \mathbf{u}_{,1},
\end{aligned} \tag{4}$$

where a superscript t denotes the transpose of a matrix or vector, c_{ijkl} represent components of the 3D elasticity tensor, a body force vector $\tilde{\mathbf{b}} = \lfloor \tilde{b}_1 \, \tilde{b}_2 \, \tilde{b}_3 \rfloor^t$, and a displacement vector $\mathbf{u} = \lfloor u_1 \, u_2 \, u_3 \rfloor^t$. The stress and strain tensors are expressed in the vector form

$$\begin{aligned}
\varepsilon &= \lfloor \, \varepsilon_{11} \quad \varepsilon_{22} \quad \varepsilon_{33} \quad 2\varepsilon_{23} \quad 2\varepsilon_{13} \quad 2\varepsilon_{12} \, \rfloor^t, \\
\sigma &= \lfloor \, \sigma_{11} \quad \sigma_{22} \quad \sigma_{33} \quad \sigma_{23} \quad \sigma_{13} \quad \sigma_{12} \, \rfloor^t.
\end{aligned} \tag{5}$$

The linear differential operator $\mathcal{L}_{23}$ and linear operator $\mathcal{L}_1$ are defined as

$$\mathcal{L}_{23} = \begin{bmatrix} 0 & 0 & 0 \\ 0 & ()_{,2} & 0 \\ 0 & 0 & ()_{,3} \\ 0 & ()_{,3} & ()_{,2} \\ ()_{,3} & 0 & 0 \\ ()_{,2} & 0 & 0 \end{bmatrix}, \quad \mathcal{L}_1 = \begin{bmatrix} 1 & 0 & 0 \\ 0 & 0 & 0 \\ 0 & 0 & 0 \\ 0 & 0 & 0 \\ 0 & 0 & 1 \\ 0 & 1 & 0 \end{bmatrix}, \tag{6}$$

in which $()_{,i} = \frac{\partial()}{\partial y_i}$.

The boundary conditions considered herein are given as follows: the lateral surface is subject to the traction such that

$$\sigma_{ij} n_j = \tilde{g}_i \quad \text{on } \partial S \times [0, l], \tag{7}$$

where $\mathbf{n}$ is the normal unit vector to the lateral surface. The ends of a beam are subject to either the traction

$$\sigma_{ij} n_j^{\sigma} = \tilde{p}_i \quad \text{on } S_\sigma = S \times \{0\}_\sigma \text{ or } S \times \{l\}_\sigma \tag{8}$$

or the prescribed displacement

$$\mathbf{u} = \bar{\mathbf{u}} \quad \text{on } S_u = S \times \{0\}_u \text{ or } S \times \{l\}_u, \tag{9}$$

in which $\mathbf{n}^\sigma$ is the normal unit vector to the end surface of a beam.

The order of magnitude of the body forces and applied forces, which yields the behavior of a beam (Cimetiere et al., 1988; Buannic and Cartraud, 2001a; Irago and Viãno, 2002), is presupposed as follows:

$$\begin{aligned} &\tilde{b}_1(x_i) = \epsilon b_1(y_i), \quad \tilde{b}_2(x_i) = \epsilon^2 b_2(y_i), \quad \tilde{b}_3(x_i) = \epsilon^2 b_3(y_i), \\ &\tilde{g}_1(x_i) = \epsilon^2 g_1(y_i), \quad \tilde{g}_2(x_i) = \epsilon^3 g_2(y_i), \quad \tilde{g}_3(x_i) = \epsilon^3 g_3(y_i), \\ &\tilde{p}_1(x_i) = \epsilon p_1(y_i), \quad \tilde{p}_2(x_i) = \epsilon^2 p_2(y_i), \quad \tilde{p}_3(x_i) = \epsilon^2 p_3(y_i). \end{aligned} \tag{10}$$

There are two different scales associated with the displacement, which are related to convergence results of the asymptotic method and are well discussed in the work of Buannic and Cartraud (2001a). Here we adopt the following scale of the displacement used in references Kolpakov (1991), Fan and Widera (1992), and Buannic and Cartraud (2000),

$$\mathbf{u}(x_i) = \mathbf{u}^{(0)}(y_1) + \sum_{n=1}^{\infty} \epsilon^n \mathbf{u}^{(n)}(y_i), \tag{11}$$

where $\mathbf{u}^{(0)} = \begin{bmatrix} 0 & u_2^{(0)} & u_3^{(0)} \end{bmatrix}^t$ and $\mathbf{u}^{(n)} = \begin{bmatrix} u_1^{(n)} & u_2^{(n)} & u_3^{(n)} \end{bmatrix}^t$. By plugging the preceding displacement into the stress and strain, their asymptotic expansions are now read as:

$$\begin{aligned} \varepsilon(x_i) &= \varepsilon^{(0)}(y_i) + \sum_{n=1}^{\infty} \epsilon^n \varepsilon^{(n)}(y_i), \\ \sigma(x_i) &= \sigma^{(0)}(y_i) + \sum_{n=1}^{\infty} \epsilon^n \sigma^{(n)}(y_i). \end{aligned} \tag{12}$$

2.2. Recursive formulation of the problem and fundamental solution

In this subsection, the recursive formulations, which include the equilibrium equations, applied loadings and boundary conditions given in the previous subsection, are presented. By substituting Eqs. (10) and (11) into Eqs. (4), (7), and (8) and collecting the same order of the small parameter ϵ, one can obtain a set of the recursive equations as follows:

$$\begin{cases} \mathcal{L}_{23}^t \sigma^{(k+1)} = -\mathcal{L}_1^t \sigma_{,1}^{(k)} - \mathbf{b}^{(k)}, \\ \varepsilon^{(k+1)} = \mathcal{L}_{23}\mathbf{u}^{(k+2)} + \mathcal{L}_1 \mathbf{u}_{,1}^{(k+1)}, \\ \sigma^{(k+1)} = \mathbf{C}\varepsilon^{(k+1)}, \\ \sigma_{ij}^{(k+1)} n_j = g_i^{(k+1)} \quad \text{on } \partial S \times [0, l], \end{cases} \qquad k \geqslant -1, \tag{13}$$

in which $\mathbf{b}^{(k)}$ and $g_i^{(k+1)}$ vanish unless $k = 1$ or 2, and boundary conditions at both ends of a beam are given by

$$\begin{cases} \mathbf{u}^{(k+1)} = \bar{\mathbf{u}}^{(k+1)} \quad \text{on } S_u, \\ \sigma_{ij}^{(k+1)} n_j^{\sigma} = p_i^{(k+1)} \quad \text{on } S_\sigma, \end{cases} \quad k \geqslant -1, \tag{14}$$

where $p_i^{(k)} = 0$ if $k \neq 1$ or 2, and $\bar{\mathbf{u}}^{(0)} = \lfloor 0 \quad \bar{u}_2 \quad \bar{u}_3 \rfloor^t$, $\bar{\mathbf{u}}^{(1)} = \lfloor \bar{u}_1 \quad 0 \quad 0 \rfloor^t$ and $\bar{\mathbf{u}}^{(k)} = 0$, $k \geqslant 1$ (Buannic and Cartraud, 2001a). Here it is worth while to mention that the treatment of displacement boundary conditions is not trivial. In general, there is no way to strictly satisfy them without obtaining the boundary layer solutions (Duva and Simmonds, 1991). This will be discussed in Section 5.

The first microscopic 2D problem, which corresponds to $k = -1$, has an analytical form of solutions, because $\sigma^{(0)} = 0$ (Buannic and Cartraud, 2000, 2001a). The next order displacement can be now found from the strain–displacement relation such that

$$\varepsilon^{(0)} = \mathcal{L}_{23}\mathbf{u}^{(1)} + \mathcal{L}_1 \mathbf{u}_{,1}^{(0)} = 0, \tag{15}$$

which renders

$$\mathbf{u}_p^{(1)} = -\lfloor 1 \quad 0 \quad 0 \rfloor^t \left(y_2 u_{2,1}^{(0)} + y_3 u_{3,1}^{(0)} \right). \tag{16}$$

The solution of the microscopic problem is defined up to a rigid body displacement ($\mathbf{u}_R$). This forms the fundamental solution such that

$$\tilde{\mathbf{u}}^{(1)}(y_i) = \mathbf{u}_p^{(1)}(y_i) + \mathbf{u}_R^{(1)}(y_i) = \Theta(y_2, y_3)\tilde{\mathbf{v}}^{(1)}(y_1) \equiv \mathbf{u}^{(1)}(y_i), \tag{17}$$

where $\mathbf{u}_R^{(1)}(y_i) = \Psi(y_2, y_3)\mathbf{v}^{(1)}(y_1)$, which has the property such that $\mathcal{L}_{23}\mathbf{u}_R = 0$,

$$\Psi(y_2, y_3) = \begin{bmatrix} 1 & 0 & 0 & 0 \\ 0 & 1 & 0 & -y_3 \\ 0 & 0 & 1 & y_2 \end{bmatrix}, \quad \Theta(y_2, y_3) = \begin{bmatrix} 1 & 0 & 0 & 0 & -y_2 & -y_3 \\ 0 & 1 & 0 & -y_3 & 0 & 0 \\ 0 & 0 & 1 & y_2 & 0 & 0 \end{bmatrix}, \tag{18}$$

and

$$\mathbf{v}^{(1)}(y_1) = \left\lfloor u_1^{(1)} \quad u_2^{(1)} \quad u_3^{(1)} \quad \phi^{(1)} \right\rfloor^t, \quad \tilde{\mathbf{v}}^{(1)}(y_1) = \left\lfloor \mathbf{v}^{(1)t} \quad u_{2,1}^{(0)} \quad u_{3,1}^{(0)} \right\rfloor^t.$$

As shown in Eq. (15), this fundamental solution does not produce any deformation on the cross-section. In other words, it explains six fundamental behaviors of the beam with the rigid cross-section and is used to kinematically correct the end effects as well as to derive the 1D macroscopic equations, which will be discussed in Section 4.

3. Microscopic 2D problems via finite element method

In this section, we seek the solution of microscopic 2D problems with the aid of the finite element method. A way to overcome the singularity of cross-sectional matrices is described, and the solution of higher than third microscopic problem is generalized. Thus one can obtain the higher-order cross-sectional deformation mode neither by solving the 3D problem nor by considering the complicated 1D beam boundary conditions. This can provide us the in-depth understanding of the 3D behavior of a beam as well as the physical insight.

3.1. Solution of the second microscopic problem

Now let us consider the second microscopic problem that corresponds to $k = 0$ in Eq. (13). The solution of the second microscopic problem, $\mathbf{u}^{(2)}$, can be decomposed into two parts as

$$\mathbf{u}^{(2)}(y_i) = \tilde{\mathbf{u}}^{(2)}(y_i) + \mathbf{u}_w^{(2)}(y_i), \tag{19}$$

where the first term consists of a trivial solution (i.e., the fundamental solution) and the second term represents a nontrivial solution accounting for the cross-sectional deformation or the warping function.

A nontrivial solution should be now sought via the virtual work concept with traction-free cross-sectional boundary conditions. The virtual work form of the second microscopic problem can be expressed as follows:

$$\int_S \delta\mathbf{u}^{(2)t}\mathcal{L}_{23}^t\sigma^{(1)}\,\mathrm{d}S = 0. \tag{20}$$

By applying the integration by parts and considering the cross-sectional boundary conditions via the divergence theorem, one can obtain

$$\underline{\int_S \delta(\mathcal{L}_{23}\tilde{\mathbf{u}}^{(2)})^t\sigma^{(1)}\,\mathrm{d}S} + \int_S \delta(\mathcal{L}_{23}\mathbf{u}_w^{(2)})^t\sigma^{(1)}\,\mathrm{d}S = 0, \tag{21}$$

where the underlined term provides the part of macroscopic equations that will be shown in Section 4.

To solve the second term given in Eq. (21), one needs to calculate the strain first. Substituting Eq. (19) into the first-order strain yields the following expression:

$$\varepsilon^{(1)} = \mathcal{L}_1\Phi(y_2,y_3)\mathbf{e}^{(1)} + \mathcal{L}_{23}\mathbf{u}_w^{(2)}, \tag{22}$$

where $\mathbf{e}^{(1)} = \begin{bmatrix} u_{1,1}^{(1)} & u_{2,11}^{(0)} & u_{3,11}^{(0)} & \phi_{,1}^{(1)} \end{bmatrix}^t$,

$$\Phi(y_2,y_3) = \begin{bmatrix} 1 & -y_2 & -y_3 & 0 \\ 0 & 0 & 0 & -y_3 \\ 0 & 0 & 0 & y_2 \end{bmatrix}. \tag{23}$$

Here one can see that the first-order strain $\varepsilon^{(1)}$ includes the classical beam strain measure $\mathbf{e}^{(1)}$ that consists of an extensional strain, two bending curvatures and a torsional strain. A similar expression can be found in Buannic and Cartraud (2000, 2001a).

3.2. Finite element discretization of the second microscopic problem

The finite element discretization is now applied to the second term in Eq. (21) using the QM6 element developed by Taylor et al. (1976). This element is based on the standard four-noded isoparametric shape functions, in which the displacement related to the strain includes the incompatible function to improve the performance, and the integration rule is modified to pass the patch test. The warping solution is then discretized as follows:

$$\mathbf{u}_w = \mathbf{N}_u\bar{\mathbf{u}}_w, \tag{24}$$

where N_u is the shape function matrix, and $\bar{\mathbf{u}}_w$ is the nodal vector.

The discretized linear system equations are obtained by plugging Eq. (24) into Eqs. (21) and (22).

$$\mathbf{K}\bar{\mathbf{u}}_w^{(2)} + \mathbf{F}_{23E}\mathbf{e}^{(1)} = \mathbf{0}, \tag{25}$$

where the matrices are defined by

$$\mathbf{K} = \langle(\mathcal{L}_{23}\mathbf{N}_u)^t\mathbf{C}(\mathcal{L}_{23}\mathbf{N}_u)\rangle, \quad \mathbf{F}_{23E} = \langle(\mathcal{L}_{23}\mathbf{N}_u)^t\mathbf{C}(\mathcal{L}_1\Phi)\rangle. \tag{26}$$

The preceding equation should be solved under the constraints such that

$$\int_S (\delta\mathbf{u}_w^{(2)})^t\cdot\mathbf{u}_R\,\mathrm{d}S = 0, \tag{27}$$

because the warping solution on the cross-section should be orthogonal to the rigid body displacement. To this end, the rigid displacement $\mathbf{u}_R$ is discretized by $\Psi = \mathbf{N}_u\overline{\Psi}$. Substituting it into Eq. (27) yields

$$(\delta\bar{\mathbf{u}}_w^{(2)})^t\mathbf{H}\overline{\Psi}\mathbf{v} = 0, \tag{28}$$

where $\mathbf{H} = \int_S \mathbf{N}_u^t\mathbf{N}_u\,\mathrm{d}S$.

By combining Eqs. (25) and (28), one can obtain

$$\mathbf{K}\bar{\mathbf{u}}_w^{(2)} + \mathbf{F}_{23E}\mathbf{e}^{(1)} = \mathbf{H}\overline{\Psi}\mathbf{v}, \tag{29}$$

where $\mathbf{v}$ can be regarded as the Lagrange multipliers, which represents the magnitude of rigid body modes and has the similar meaning as μ in Cesnik et al. (1996). Multiplying Eq. (29) by $\overline{\Psi}^t$ yields

$$\mathbf{v} = (\overline{\Psi}^t\mathbf{H}\overline{\Psi})^{-1}\overline{\Psi}^t\left(\mathbf{K}\bar{\mathbf{u}}_w^{(2)} + \mathbf{F}_{23E}\mathbf{e}^{(1)}\right). \tag{30}$$

causes Eq. (29) to become

$$\widetilde{\mathbf{I}}\left(\mathbf{K}\bar{\mathbf{u}}_w^{(2)} + \mathbf{F}_{23E}\mathbf{e}^{(1)}\right) = \mathbf{0}, \tag{31}$$

where $\widetilde{\mathbf{I}} = \{\mathbf{I} - \mathbf{H}\overline{\Psi}(\overline{\Psi}^t\mathbf{H}\overline{\Psi})^{-1}\overline{\Psi}^t\}$. Note that the matrix $\widetilde{\mathbf{I}}$ cannot be simply eliminated since it is a singular matrix.

The matrix $\widetilde{\mathbf{I}}\mathbf{K}$ still possesses four zero eigenvalues which correspond to the rigid body modes (three translations and one rotation on the cross-section). There are two methods to remove them; one is to apply four point constraints (Giavotto et al., 1983; Cesnik et al., 1996), and the other is to apply the penalty function based on eigenvectors corresponding to zero eigenvalues (Peters and Hackl, 2005). Here we adopt the latter one since it is numerically efficient and such eigenvectors are already known (i.e., $\overline{\Psi}$). One can rewrite Eq. (31) as:

$$\widehat{\mathbf{K}}\bar{\mathbf{u}}_w^{(2)} = -\widetilde{\mathbf{I}}\mathbf{F}_{23E}\mathbf{e}^{(1)}, \tag{32}$$

in which $\widehat{\mathbf{K}} = (\widetilde{\mathbf{I}}\mathbf{K} + \alpha\overline{\Psi}\overline{\Psi}^t)$, where α is the penalty parameter which can be systematically determined via an eigenvalue analysis, i.e., the largest eigenvalue of the matrix, $\widetilde{\mathbf{I}}\mathbf{K}$.

Consequently the solution of Eq. (32) is represented by

$$\bar{\mathbf{u}}_w^{(2)} = \Gamma_e^{(1)}\mathbf{e}^{(1)}, \tag{33}$$

where

$$\Gamma_e^{(1)} = -\widehat{\mathbf{K}}^{-1}\widetilde{\mathbf{I}}\mathbf{F}_{23E}. \tag{34}$$

Note that each column of $\Gamma_e^{(1)}$ corresponds to four cross-sectional deformations such as extension, two bending and torsion. In general, for an isotropic beam with a solid cross-section, extension and two bending modes represent the 3D in-plane Poisson's effects, and a torsion mode represents the out-of-plane Saint–Venant's torsional warping.

3.3. Solution of the third and higher microscopic problem

Unlike first two microscopic problems, a body force vector $\mathbf{b}^{(1)}$ and a lateral surface traction vector $\mathbf{g}^{(2)}$ are presented in the third microscopic problem, $k = 1$ in Eq. (13). Here we make the assumption that these forces vary only along the axial coordinate y_1, which means that their distributions on the cross-section are constant along the coordinate y_1, so as to separate them into two functions such that

$$\begin{aligned}\mathbf{b}^{(1)}(y_i) &= \mathbf{B}^{(1)}(y_2, y_3)\hat{\mathbf{b}}^{(1)}(y_1),\\ \mathbf{g}^{(2)}(y_i) &= \mathbf{G}^{(2)}(y_2, y_3)\hat{\mathbf{g}}^{(2)}(y_1).\end{aligned} \tag{35}$$

For the solution of the third microscopic problem, $\mathbf{u}^{(3)} = \tilde{\mathbf{u}}^{(3)} + \mathbf{u}_w^{(3)}$, by applying the procedure described in Section 3.1, the virtual work form is expressed as

$$\int_S \delta(\mathcal{L}_{23}\mathbf{u}^{(3)})^t\sigma^{(2)}\,\mathrm{d}S = \int_S \delta\mathbf{u}^{(3)t}\mathcal{L}_1^t\sigma_{,1}^{(1)}\,\mathrm{d}S + \int_S \delta\mathbf{u}^{(3)t}\mathbf{B}^{(1)}\,\mathrm{d}S\hat{\mathbf{b}}^{(1)} + \int_{\partial S} \delta\mathbf{u}^{(3)t}\mathbf{G}^{(2)}\,\mathrm{d}S\hat{\mathbf{g}}^{(2)}, \tag{36}$$

where the terms related to $\delta\tilde{\mathbf{u}}^{(3)}$ contribute to the 1D macroscopic equations, and the terms related to $\delta\mathbf{u}_w^{(3)}$ form the 2D microscopic equations.

By applying the procedure described in Section 3.2 to Eq. (36), the discretized linear system equations can be obtained as follows:

$$\mathbf{K}\bar{\mathbf{u}}_w^{(3)} = -\mathbf{F}_{23E}\mathbf{e}^{(2)} + \mathbf{F}_{11E}\mathbf{e}_{,1}^{(1)} + (\mathbf{F}_{231}^t - \mathbf{F}_{231})\bar{\mathbf{u}}_{w,1}^{(2)} + \mathbf{F}_B^{(1)}\hat{\mathbf{b}}^{(1)} + \mathbf{F}_G^{(2)}\hat{\mathbf{g}}^{(2)}, \tag{37}$$

where the new matrices are defined by

$$\begin{aligned} &\mathbf{F}_{11E} = \langle(\mathcal{L}_1\mathbf{N}_u)^t\mathbf{C}(\mathcal{L}_1\Phi)\rangle, \quad \mathbf{F}_{231} = \langle(\mathcal{L}_{23}\mathbf{N}_u)^t\mathbf{C}(\mathcal{L}_1\mathbf{N}_u)\rangle, \\ &\mathbf{F}_B^{(1)} = \langle(\mathbf{N}_u)^t\mathbf{B}^{(1)}\rangle, \quad \mathbf{F}_G^{(2)} = \langle(\mathbf{N}_u)^t\mathbf{G}^{(2)}\rangle_{\partial S}, \end{aligned} \tag{38}$$

where $\langle\bullet\rangle_{\partial S} = \int_{\partial S}\bullet\,\mathrm{d}S$.

By following the same way described in Section 3.2, the solution of Eq. (37) is now represented by

$$\bar{\mathbf{u}}_w^{(3)} = \Gamma_e^{(1)}\mathbf{e}^{(2)} + \Gamma_e^{(2)}\mathbf{e}_{,1}^{(1)} + \bar{\mathbf{u}}_f^{(3)}, \tag{39}$$

where

$$\bar{\mathbf{u}}_f^{(3)} = \widetilde{\mathbf{F}}_b^{(1)}\hat{\mathbf{b}}^{(1)} + \widetilde{\mathbf{F}}_g^{(2)}\hat{\mathbf{g}}^{(2)} \tag{40}$$

and

$$\begin{aligned} &\Gamma_e^{(2)} = \widehat{\mathbf{K}}^{-1}\widetilde{\mathbf{I}}\left\{\mathbf{F}_{11E} + (\mathbf{F}_{231}^t - \mathbf{F}_{231})\Gamma_e^{(1)}\right\}, \\ &\widetilde{\mathbf{F}}_b^{(1)} = \widehat{\mathbf{K}}^{-1}\widetilde{\mathbf{I}}\mathbf{F}_B^{(1)}, \quad \widetilde{\mathbf{F}}_g^{(2)} = \widehat{\mathbf{K}}^{-1}\widetilde{\mathbf{I}}\mathbf{F}_G^{(2)}. \end{aligned} \tag{41}$$

Similarly, the warping solution of the higher than third microscopic problem is obtained by

$$\bar{\mathbf{u}}_w^{(k)} = \sum_{m=1}^{k-1}\Gamma_e^{(m)}\partial_{y_1}^{m-1}\mathbf{e}^{(k-m)} + \bar{\mathbf{u}}_f^{(k)}, \quad k \geqslant 4, \tag{42}$$

where $\Gamma_e^{(m)}$, which represents the mth order cross-sectional deformation mode, can be generalized as

$$\Gamma_e^{(m)} = \widehat{\mathbf{K}}^{-1}\widetilde{\mathbf{I}}\left\{\mathbf{F}_{11N}\Gamma_e^{(m-2)} + \left(\mathbf{F}_{231}^t - \mathbf{F}_{231}\right)\Gamma_e^{(m-1)}\right\}, \quad m \geqslant 3, \tag{43}$$

in which $\mathbf{F}_{11N}^e = \langle(\mathcal{L}_1\mathbf{N}_u)^t\mathbf{C}(\mathcal{L}_1\mathbf{N}_u)\rangle$. Thanks to Eqs. (42) and (43), the complete displacement solution of the kth microscopic problem can be now generalized by

$$\mathbf{u}^{(k)} = \Theta\tilde{\mathbf{v}}^{(k)} + \sum_{m=1}^{k-1}\mathbf{N}_u\Gamma_e^{(m)}\partial_{y_1}^{m-1}\mathbf{e}^{(k-m)} + \mathbf{N}_u\bar{\mathbf{u}}_f^{(k)}, \quad k \geqslant 1. \tag{44}$$

4. Macroscopic 1D problems

A set of macroscopic 1D beam equations can be derived from the virtual work of each microscopic problem. A fundamental solution, $\tilde{\mathbf{u}}^{(k)}$, in each microscopic problem does not produce any deformation on the cross-section as mentioned in Section 2.2. Thus the terms related to the variation of this solution should be vanished. In this way, the virtual work of each microscopic problem is equilibrated, and a set of macroscopic 1D beam equations can be derived.

4.1. Macroscopic 1D beam equilibrium equations

The term related to the variation of a fundamental solution appears first in the second microscopic problem. Recalling that $\mathcal{L}_{23}\mathbf{u}_R = 0$, one can rewrite the underline term in Eq. (21) as

$$\int_S \delta\left(\mathcal{L}_{23}\mathbf{u}_p^{(2)}\right)^t\sigma^{(1)}\,\mathrm{d}S = 0. \tag{45}$$

This becomes $\delta u_{2,1}^{(1)}\langle\sigma_{12}^{(1)}\rangle + \delta u_{3,1}^{(1)}\langle\sigma_{13}^{(1)}\rangle = 0$, which implies that

$$\left\langle\sigma_{12}^{(1)}\right\rangle \equiv Q_2^{(1)} = 0, \quad \left\langle\sigma_{13}^{(1)}\right\rangle \equiv Q_3^{(1)} = 0. \tag{46}$$

In the third microscopic problem, from Eq. (36), we have

$$\int_S \delta(\mathcal{L}_{23}\mathbf{u}_p^{(3)})^t \sigma^{(2)}\,\mathrm{d}S = \int_S \delta\tilde{\mathbf{u}}^{(3)t}\mathcal{L}_1^t\sigma_{,1}^{(1)}\,\mathrm{d}S + \int_S \delta\tilde{\mathbf{u}}^{(3)t}\mathbf{B}^{(1)}\,\mathrm{d}S\,\hat{\mathbf{b}}^{(1)} + \int_{\partial S}\delta\tilde{\mathbf{u}}^{(3)t}\mathbf{G}^{(2)}\,\mathrm{d}S\,\hat{\mathbf{g}}^{(2)}, \tag{47}$$

from which one may obtain the first set of beam equilibrium equations. There are, however, the trivial terms related to first-order shear forces $Q^{(1)}$ that are equal to zero from Eq. (46). This corresponds to the assumption usually made in a classical beam theory. In addition, first-order bending moments $M^{(1)}$ are connected to second-order shear forces $Q^{(2)}$ that are also presented in the fourth microscopic problem (Buannic and Cartraud, 2000, 2001a). This makes it possible to express the beam equilibrium equations in terms of first-order stress resultants. Thus one can obtain a set of the beam equilibrium equations corresponding to the first macroscopic 1D problem from the third and fourth microscopic problem as follows:

$$\begin{aligned} &N_{,1}^{(1)} + f_1 = 0,\\ &M_{\alpha,11}^{(1)} - m_{\alpha,1} - f_\alpha = 0,\\ &T_{,1}^{(1)} = 0, \end{aligned} \tag{48}$$

where

$$\begin{aligned} &N^{(1)} = \left\langle \sigma_{11}^{(1)} \right\rangle, \quad M_\alpha^{(1)} = -\left\langle y_\alpha \sigma_{11}^{(1)} \right\rangle, \quad T^{(1)} = \left\langle y_2\sigma_{13}^{(1)} - y_3\sigma_{12}^{(1)} \right\rangle,\\ &f_1 = \left\langle B_1^{(1)} \right\rangle \hat{b}_1^{(1)} + \left\langle G_1^{(2)} \right\rangle_{\partial S}\hat{g}_1^{(2)},\\ &f_\alpha = \langle B_\alpha^{(2)}\rangle \hat{b}_\alpha^{(2)} + \langle G_\alpha^{(3)}\rangle_{\partial S}\hat{g}_\alpha^{(3)},\\ &m_\alpha = \left\langle y_\alpha B_1^{(1)} \right\rangle \hat{b}_1^{(1)} + \left\langle y_\alpha G_1^{(2)} \right\rangle_{\partial S}\hat{g}_1^{(2)}, \end{aligned} \tag{49}$$

in which the index α varies from 2 to 3. f_1 and f_α represent the applied axial and shear forces, respectively. m_α are moments acting on the cross-section.

In the same manner, from fourth and fifth microscopic problems, the second set of beam equilibrium equations can be written as

$$N_{,1}^{(2)} = 0, \quad M_{2,11}^{(2)} = 0, \quad M_{3,11}^{(2)} = 0, \quad T_{,1}^{(2)} + \tau = 0, \tag{50}$$

where

$$\tau = \left\langle y_2 B_3^{(2)}\hat{b}_3^{(2)} - y_3 B_2^{(2)}\hat{b}_2^{(2)} \right\rangle + \left\langle y_2 G_3^{(3)}\hat{g}_3^{(3)} - y_3 G_2^{(3)}\hat{g}_2^{(3)} \right\rangle_{\partial S}. \tag{51}$$

The higher than second set of beam equilibrium equations is now generalized, since the body force and applied surface traction do not appear due to the assumptions made in Eq. (10), as follows:

$$N_{,1}^{(k)} = 0, \quad M_{2,11}^{(k)} = 0, \quad M_{3,11}^{(k)} = 0, \quad T_{,1}^{(k)} = 0, \qquad k \geqslant 3. \tag{52}$$

4.2. Macroscopic 1D beam constitutive equations

The first-order beam constitutive equations can be defined as follows:

$$\widetilde{\mathcal{N}}^{(1)} = \langle(\mathcal{L}_1\Phi)^t\sigma^{(1)}\rangle \equiv \mathcal{A}^{(1)}\mathbf{e}^{(1)}, \tag{53}$$

where $\widetilde{\mathcal{N}}^{(1)}$ and $\mathcal{A}^{(1)}$ are the 4×1 vector and the 4×4 matrix, respectively, and their explicit expressions are given by

$$\begin{aligned} &\widetilde{\mathcal{N}}^{(1)} = \lfloor N^{(1)} \quad M_2^{(1)} \quad M_3^{(1)} \quad T^{(1)} \rfloor^t,\\ &\mathcal{A}^{(1)} = \langle(\mathcal{L}_1\Phi)^t\mathbf{C}(\mathcal{L}_1\Phi)\rangle + \langle(\mathcal{L}_1\Phi)^t\mathbf{C}(\mathcal{L}_{23}\mathbf{N}_u)\rangle\Gamma_e^{(1)}. \end{aligned} \tag{54}$$

The higher than first-order beam constitutive equations, from Eq. (44), can be now generalized as follows:

$$\widetilde{\mathcal{N}}^{(k)} = \sum_{m=1}^{k} \mathcal{A}^{(m)} \partial_{y_1}^{m-1} \mathbf{e}^{(k-m+1)} + \widetilde{\mathcal{N}}_f^{(k)}, \quad k \geqslant 2, \tag{55}$$

where

$$\begin{aligned} \mathcal{A}^{(k)} &= \langle (\mathcal{L}_1 \Phi)^t \mathbf{C} (\mathcal{L}_1 \mathbf{N}_u) \rangle \Gamma_e^{(k-1)} + \langle (\mathcal{L}_1 \Phi)^t \mathbf{C} (\mathcal{L}_{23} \mathbf{N}_u) \rangle \Gamma_e^{(k)}, \\ \widetilde{\mathcal{N}}_f^{(k)} &= \langle (\mathcal{L}_1 \Phi)^t \mathbf{C} (\mathcal{L}_{23} N_u) \rangle \bar{\mathbf{u}}_f^{(k+1)}. \end{aligned} \tag{56}$$

4.3. The weak form of macroscopic 1D problems

By considering the boundary conditions given in Eq. (14), the weak form of the first beam equilibrium equations, Eq. (48), can be found as follows:

$$\int_0^l \left\{ (\delta \mathbf{e}^{(1)})^t \widetilde{\mathcal{N}}^{(1)} - (\delta \hat{\mathbf{v}}^{(1)})^t \widetilde{\mathcal{B}}^{(1)} \right\} \mathrm{d}y_1 = \left\{ (\delta \hat{\mathbf{v}}^{(1)})^t \left(\widetilde{\mathcal{F}}^{(1)} + \widetilde{\mathcal{F}}_Q^{(2)} \right) \right\}, \tag{57}$$

where

$$\begin{aligned} &\hat{\mathbf{v}}^{(1)} = \begin{bmatrix} u_1^{(1)} & u_2^{(0)} & u_3^{(0)} & \phi^{(1)} & u_{2,1}^{(0)} & u_{3,1}^{(0)} \end{bmatrix}^t, \quad \widetilde{\mathcal{B}}^{(1)} = \lfloor f_1 \quad f_2 \quad f_3 \quad 0 \quad m_2 \quad m_3 \rfloor^t, \\ &\widetilde{\mathcal{F}}^{(1)} = \langle \Theta^t(y_2, y_3) \lfloor p_1 \quad 0 \quad 0 \rfloor^t \rangle, \quad \widetilde{\mathcal{F}}_Q^{(2)} = \lfloor 0 \quad \langle p_2 \rangle \quad \langle p_3 \rangle \quad 0 \quad 0 \quad 0 \rfloor^t, \end{aligned} \tag{58}$$

in which Θ is given in Eq. (18). An applied force vector, $\widetilde{\mathcal{F}}^{(1)}$, includes a tensile force and two bending moments related to $\sigma^{(1)}$, whereas $\widetilde{\mathcal{F}}_Q^{(2)}$ includes two shear forces related to $\sigma^{(2)}$. It should be noticed that there is no applied torsion in this macroscopic problem that will be presented in the second macroscopic problem. Thus the torsion angle $\phi^{(1)}(y_1) = 0$ unless there exist tension–torsion and/or bending–torsion couplings.

The weak from of the second beam equilibrium equations, Eq. (50), is given by

$$\int_0^l \left\{ (\delta \mathbf{e}^{(2)})^t \widetilde{\mathcal{N}}^{(2)} - (\delta \hat{\mathbf{v}}^{(2)})^t \widetilde{\mathcal{B}}^{(2)} \right\} \mathrm{d}y_1 = \left\{ (\delta \hat{\mathbf{v}}^{(2)})^t \widetilde{\mathcal{F}}_T^{(2)} \right\}, \tag{59}$$

where

$$\begin{aligned} &\hat{\mathbf{v}}^{(2)} = \begin{bmatrix} u_1^{(2)} & u_2^{(1)} & u_3^{(1)} & \phi^{(2)} & u_{2,1}^{(1)} & u_{3,1}^{(1)} \end{bmatrix}^t, \\ &\widetilde{\mathcal{B}}^{(2)} = \lfloor 0 \quad 0 \quad 0 \quad \tau \quad 0 \quad 0 \rfloor^t, \quad \widetilde{\mathcal{F}}_T^{(2)} = \lfloor 0 \quad 0 \quad 0 \quad \langle y_2 p_3 - y_3 p_2 \rangle \quad 0 \quad 0 \rfloor^t. \end{aligned} \tag{60}$$

Unlike first two macroscopic problems, the weak form of the higher than second beam equilibrium equations, Eq. (52), can be generalized, since there are no body forces and applied forces, as follows:

$$\int_0^l (\delta \mathbf{e}^{(k)})^t \widetilde{\mathcal{N}}^{(k)} \, \mathrm{d}y_1 = 0, \quad k \geqslant 3. \tag{61}$$

Here it should be mentioned that the beam formulations (weak form) presented in the above are different from those (strong form) reported in the literature (Duva and Simmonds, 1991; Buannic and Cartraud, 2001b). The weak formulation has a merit in that the force boundary conditions are automatically handled.

Each weak form of beam equilibrium equations presented in Eqs. (57), (59) and (61), is discretized by using three-noded finite beam elements, in which quadratic Lagrangian and fifth-order Hermite interpolation functions are used for $(u_1^{(k)}, \phi^{(k)})$ and $(u_2^{(k)}, u_3^{(k)})$, respectively. The interpolation functions used herein are selected to provide the accurate higher-order derivatives, up to the fourth-order one, with respect to the coordinate y_1. Then one can obtain the kth order beam equations as follows:

$$\mathbf{K}_b^{(1)} \widehat{\mathbf{V}}^{(k)} = -\mathbf{P}_N^{(k)} + \mathbf{P}_F^{(k)}, \quad k \geqslant 1, \tag{62}$$

where the first-order beam stiffness matrix $\mathbf{K}_b^{(1)}$, the kth order nodal degrees of freedom vector $\widehat{\mathbf{V}}^{(k)}$, and the kth order force vector $\mathbf{P}^{(k)}$ are given by

$$\begin{aligned}\mathbf{K}_b^{(k)} &= \int_0^l (\mathcal{L}_b^{(1)}\mathbf{N}_b)^t \mathcal{A}^{(k)} (\mathcal{L}_b^{(k)}\mathbf{N}_b)\mathrm{d}y_1,\\ \mathbf{P}_N^{(k)} &= \sum_{m=2}^{k} \mathbf{K}_b^{(m)} \widehat{\mathbf{V}}^{(k-m+1)} + \int_0^l (\mathcal{L}_b^{(1)}\mathbf{N}_b)^t \widetilde{\mathcal{N}}_f^{(k)}\,\mathrm{d}y_1,\end{aligned} \tag{63}$$

in which $\mathbf{N}_b$ is the beam shape function matrix, $\mathcal{L}_b^{(1)}$ is the linear differential operator for a beam, and $\mathcal{L}_b^{(k)} = \partial_{y_1}^{(k-1)}\mathcal{L}_b^{(1)},\ k \geqslant 2$. The fictive volume force, $\mathbf{P}_N^{(k)}$, which accounts for the higher-order effects (Buannic and Cartraud, 2001a). A beam force vector $\mathbf{P}_F^{(k)}$ is given by

$$\begin{aligned}\mathbf{P}_F^{(1)} &= \int_0^l (\mathbf{N}_b)^t \widetilde{\mathcal{B}}^{(1)}\,\mathrm{d}y_1 + \left\{(\mathbf{N}_b)^t(\widetilde{\mathcal{F}}^{(1)} + \widetilde{\mathcal{F}}_Q^{(2)})\right\},\\ \mathbf{P}_F^{(2)} &= \int_0^l (\mathbf{N}_b)^t \widetilde{\mathcal{B}}^{(2)}\,\mathrm{d}y_1 + \left\{(\mathbf{N}_b)^t \widetilde{\mathcal{F}}_T^{(2)}\right\},\end{aligned} \tag{64}$$

and $\mathbf{P}_F^{(k)} = \mathbf{0},\ k \geqslant 3$.

5. Boundary conditions

The weak form presented in Section 4.3 provides the displacement boundary conditions at the end of a beam, $\delta\hat{\mathbf{v}} = 0$, which indicates that six fundamental displacements must be prescribed. It, however, does not tell us how such displacements are prescribed. As discussed in Duva and Simmonds (1991) and Duva and Simmonds (1992), it is not trivial to satisfy the 3D displacement boundary conditions given in Eq. (9). One can obtain asymptotically correct boundary conditions without solving boundary layer problems by applying the decay analysis method proposed by Gregory and Wan (1984). This method was successfully applied to a sandwich beam (Buannic and Cartraud, 2000) and periodic heterogeneous beams (Buannic and Cartraud, 2001b) as well as isotropic or orthotropic beams (Gregory and Wan, 1984; Duva and Simmonds, 1991; Fan and Widera, 1992). It is, however, too difficult to obtain asymptotically correct boundary conditions, which have turned out to be different from those derived by variational principles for a displacement prescribed boundary (Fan and Widera, 1994), via this decay method for engineering applications in general. Thus one needs to simplify these boundary conditions while providing accurate enough results to engineering applications. Such simplified boundary conditions were obtained by Horgan and Simmonds (1991) for a transversely isotropic semi-infinite beam and were applied to a linear vibration analysis of orthotropic cantilevered beams (Duva and Simmonds, 1992). Horgan and Simmonds (1991) derived the necessary conditions to decay for four sets of boundary conditions, such as traction, mixed (two) and displacement, as $\epsilon \to 0$, where ϵ is the ratio of the shear modulus to the geometric mean of axial and transverse moduli. In fact, these simplified boundary conditions are equivalent to so-called *averaged displacement* boundary conditions for a clamped boundary (Savoia and Tullini, 1996). In this paper, these are generalized by employing the orthogonality conditions of asymptotic displacements to six fundamental solutions as constraints.

The displacement boundary conditions given in Eq. (9) can be interpreted as constraint equations. One can express them in the weak form

$$\int_{S_u} (\delta\tilde{\mathbf{u}}^{(k)})^t(\mathbf{u}^{(k)} - \bar{\mathbf{u}}^{(k)})\,\mathrm{d}S = 0, \quad k \geqslant 1, \tag{65}$$

where $u_\alpha^{(0)} = \bar{u}_\alpha$ from Eq. (14), and substituting Eq. (17) into the above yields

$$(\delta\tilde{\mathbf{v}}^{(k)})^t\mathbf{U}^{(k)} = 0, \quad \mathbf{U}^{(k)} \equiv \int_{S_u} \Theta^t(y_2, y_3)(\mathbf{u}^{(k)} - \bar{\mathbf{u}}^{(k)})\,\mathrm{d}S, \tag{66}$$

where $\mathbf{U}^{(k)}$ is a 6×1 vector, and the matrix Θ related to six fundamental solutions is given in Eq. (18). Similar constraint equations can be found in flexible multibody dynamics (Simeon, 2006).

Since the necessary conditions to decay for the mixed data are the same as those for the displacement data (Horgan and Simmonds, 1991), four sets of boundary conditions can be generalized as follows:

- Case (A), stress data:

$$\left\lfloor N^{(1)} \quad M_2^{(1)} \quad M_3^{(1)} \right\rfloor^t = \left\langle \Theta^t \lfloor p_1 \quad 0 \quad 0 \rfloor^t \right\rangle, \quad Q_\alpha^{(2)} = \langle p_\alpha \rangle, \quad T^{(2)} = \langle y_2 p_3 - y_3 p_2 \rangle. \tag{67}$$

- Case (B), mixed data:

$$Q_\alpha^{(2)} = \langle p_\alpha \rangle, \quad T^{(2)} = \langle y_2 p_3 - y_3 p_2 \rangle, \quad \mathbf{U}_{(1,5,6)}^{(k)} = 0. \tag{68}$$

- Case (C), mixed data:

$$\left\lfloor N^{(1)} \quad M_2^{(1)} \quad M_3^{(1)} \right\rfloor^t = \left\langle \Theta^t \lfloor p_1 \quad 0 \quad 0 \rfloor^t \right\rangle, \quad \mathbf{U}_{(2:4)}^{(k)} = 0. \tag{69}$$

- Case (D), displacement data:

$$\mathbf{U}_{(1:6)}^{(k)} = 0. \tag{70}$$

In the above, the simply supported boundary conditions are equivalent to Case (C). This is the case that the higher-order effect (e.g., the transverse shear deformation) purely comes from the fictive volume force, since there is no edge effect.

Once we solved the beam equations of Eq. (62) along with the boundary conditions of Eqs. (67)–(70), one can recover 3D displacements and stresses on the cross-section at any axial locations by using Eqs. (11) and (12).

We shall henceforth focus on the clamped boundary conditions ($\bar{\mathbf{u}}^{(k)} = \mathbf{0},\ k \geqslant 0$) since the displacement boundary conditions only are problematic, as discussed in Fan and Widera (1994). One can express them in the recursive manner by substituting Eq. (44) into Eq. (66) as follows:

$$\begin{aligned}
&\tilde{\mathbf{v}}^{(1)}(0) = \mathbf{0},\\
&\tilde{\mathbf{v}}^{(2)}(0) = -\mathbf{H}_\theta^{-1} \langle \Theta^t \mathbf{N}_u \rangle \Gamma_e^{(1)} \mathbf{e}^{(1)}|_0,\\
&\tilde{\mathbf{v}}^{(k)}(0) = -\mathbf{H}_\theta^{-1} \langle \Theta^t \mathbf{N}_u \rangle \left(\sum_{m=1}^{k-1} \Gamma_e^{(m)} \partial_{y_1}^{m-1} \mathbf{e}^{(k-m)} + \bar{\mathbf{u}}_f^{(k)} \right)\Bigg|_0, \quad k \geqslant 3,
\end{aligned} \tag{71}$$

where $\mathbf{H}_\theta = \langle \Theta^t \Theta \rangle$. Note that the displacement boundary conditions presented in the above should be rearranged by corresponding components to the macroscopic 1D problems. The beam displacement boundary conditions $\hat{\mathbf{v}}^{(k)}(0)$ can be now represented by

$$\begin{aligned}
&\hat{\mathbf{v}}^{(1)}(0) = \mathbf{0},\\
&\hat{\mathbf{v}}^{(k)}(0) = \left\lfloor \tilde{\mathbf{v}}_1^{(k)} \quad \tilde{\mathbf{v}}_2^{(k-1)} \quad \tilde{\mathbf{v}}_3^{(k-1)} \quad \tilde{\mathbf{v}}_4^{(k)} \quad \tilde{\mathbf{v}}_5^{(k)} \quad \tilde{\mathbf{v}}_6^{(k)} \right\rfloor^t\Big|_0, \quad k \geqslant 2.
\end{aligned} \tag{72}$$

6. Numerical examples and discussions

A sandwich beam with a solid cross-section and composite beams with closed thin-walled cross-sections are considered in this study. The results obtained herein are compared to those available in literature to assess the accuracy of the formal asymptotic beam analysis with proposed displacement boundary conditions. The present approach is referred to as FAMBA (Formal Asymptotic Method-based Beam Analysis) throughout numerical examples.

In all figures reported herein, the zeroth-, first-, and second-order solutions are represented by the beam displacement vector such that

$$\hat{\mathbf{u}}^{(k-1)}(y_1) \equiv \hat{\mathbf{v}}^{(k)}(y_1) = \left\lfloor u_1^{(k)} \quad u_2^{(k-1)} \quad u_3^{(k-1)} \quad \phi^{(k)} \quad u_{2,1}^{(k-1)} \quad u_{3,1}^{(k-1)} \right\rfloor, \tag{73}$$

where $\hat{\mathbf{u}}^{(k-1)}$, $k \geqslant 1$, represent the $(k-1)$th order beam solutions. The zeroth-order solutions correspond to the classical Euler–Bernoulli–Navier beam theory, and first-order and/or second-order solutions are comparable to the Rankine–Timoshenko beam theory.

In what follows, it will be demonstrated that the boundary conditions given in Eq. (73) are simple enough for engineering applications and accurate enough for high precision analyses, as long as the interior solutions are concerned. In some of reported figures, 3D FEM results are obtained by using hybrid stress eight-noded brick elements developed by Yeo and Lee (1997) in order to save the computational efforts.

6.1. A sandwich beam with a solid cross-section

An example considered in this subsection is taken from Buannic and Cartraud (2000), where a cantilevered sandwich beam with a square solid cross-section was analyzed by applying the boundary conditions obtained from the decay analysis based on the Maxwell–Betti's reciprocal theorem. The beam dimension is shown in Fig. 2 and the material properties of face sheets are $E = 200$ GPa and $v = 0.3$, and those of a core are $E = 0.4$ GPa and $v = 0.3$.

The bending deflection and slope of a sandwich beam under a vertical unit tip load are shown in Fig. 3, where the axial coordinate is normalized by the length of a beam, 300 mm. The results of 3D FEM are obtained by using 14,000 solid elements. The first-order solution is found to be zero because there are no couplings, whereas the second-order solution shows a significant improvement with non-zero slope boundary condition at the clamped end. The present zeroth- and second-order solutions are the same as those given in Buannic and Cartraud (2000). In fact, the third-order solution recovers the 3D interior solution with the aid of the decay method, as demonstrated in Buannic and Cartraud (2000). At this point, it should be noticed

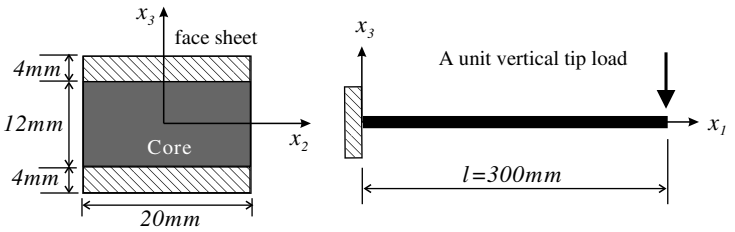

Fig. 2. Geometry of a sandwich beam cross-section.

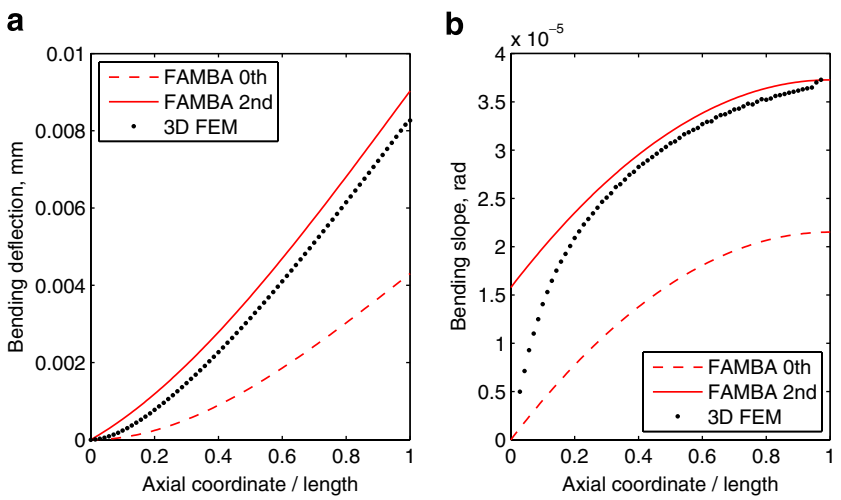

Fig. 3. A sandwich beam under a vertical unit tip load: (a) bending deflection and (b) bending slope.

that such third-order correction could not be achieved with the displacement orthogonality conditions presented in Eq. (66) which could produce comparable results to the Rankine–Timoshenko beam theory (Duva and Simmonds, 1991; Duva and Simmonds, 1992).

In Figs. 4 and 5, the first- and second-order cross-sectional deformation modes of a sandwich beam are illustrated, which correspond to $\Gamma_e^{(1)}$ and $\Gamma_e^{(2)}$ given in Eqs. (34) and (41). In Fig. 4, one can see the 3D Poisson's effects for extension and two bending modes, which are usually neglected in beam theories, and the Saint–Venant's warping for a torsion mode. The non-classical cross-sectional deformations appear at the second-order warping solution $\Gamma_e^{(2)}$, as shown in Fig. 5. One can clearly see the shear deformation effects in two bending modes and the in-plane cross-sectional distortion in a torsion mode. These cross-sectional deformation modes, which can be calculated without solving beam problems using Eq. (43) for kth order, enable us to have a physical insight on the 3D behavior of a beam.

In order to illustrate the asymptotic behavior of the FAMBA, the tip deflections of a sandwich beam with the same cross-sectional dimension are presented in Fig. 6. The tip deflection is normalized so that the zeroth-order solution yields a constant value irrespective of the length-to-thickness ratio S. This sandwich beam exhibits a significant shear deformation due to the flexible core material. The zeroth-order solution is, therefore, very poor as $S \geqslant 50$, whereas the second-order solution is well correlated with the 3D FEM solution.

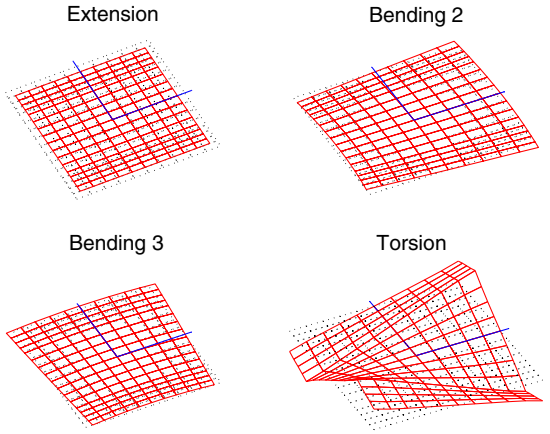

Fig. 4. The first-order cross-sectional deformation mode of a sandwich beam, $\Gamma_e^{(1)}$.

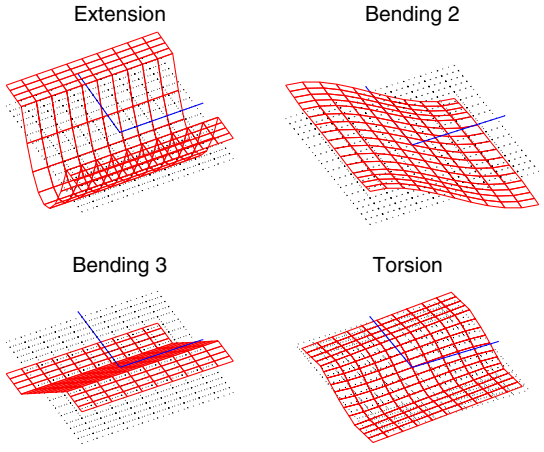

Fig. 5. The second-order cross-sectional deformation mode of a sandwich beam, $\Gamma_e^{(2)}$.

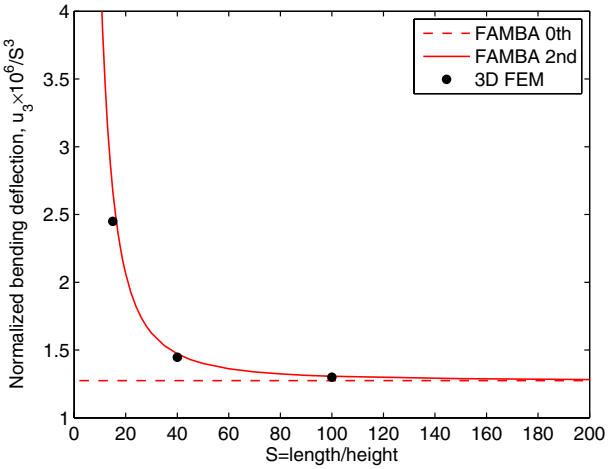

Fig. 6. Tip deflection of a sandwich beam with varying length-to-height ratio.

6.2. Thin-walled composite box beams

In this subsection, cantilevered thin-walled composite beams are considered to compare the results obtained herein with those available in literature. A thin-walled box beam configuration is shown in Fig. 7, where the height $h_3 = 13.46$ mm (0.53 in.), the width $h_2 = 24.2$ mm (0.953 in.), the wall thickness $t = 0.762$ mm (0.03 in.), and the length $l = 762$ mm (30 in.). The ply material properties of AS4/3501-6 graphite-epoxy are taken from Chandra et al. (1990) and Kim and White (1997).

$$\begin{aligned} &E_L = 141.96\ \text{GPa}\ (20.59 \times 10^6\ \text{psi}), \quad E_T = 9.79\ \text{GPa}\ (1.42 \times 10^6\ \text{psi}),\\ &G_{LT} = 6.0\ \text{GPa}\ (0.87 \times 10^6\ \text{psi}), \quad G_{TT} = 4.83\ \text{GPa}\ (0.69 \times 10^6\ \text{psi}),\\ &\nu_{LT} = \nu_{TT} = 0.42, \quad \text{ply thickness} = 0.127\ \text{mm}\ (0.005\ \text{in.}), \end{aligned} \tag{74}$$

where L and T denote a fiber direction and a perpendicular direction to the fiber, respectively.

Four cases are considered in this subsection, which are listed in Table 1. The orthotropic box beam (Case 1) is taken from Popescu and Hodges (2000). The circumferentially uniform stiffness (CUS) configuration or the antisymmetric configuration (Case 2) and the circumferentially asymmetric stiffness (CAS) configuration or the symmetric configuration (Cases 3 and 4) are taken from Chandra et al. (1990) and Kim and White (1997). For all cases, either the shear force or tensile force of 4.448 N (1 lb) is applied at the free end of a beam. For a CUS1 configuration, the results of 3D FEM are obtained by using 2400 solid elements.

6.2.1. An orthotropic box beam

An orthotropic box beam (Case 1) is analyzed first. In Fig. 8, normalized deflections are plotted as a function of length-to-height ratio, where VABS and NABSA results are reproduced by taking their stiffness from

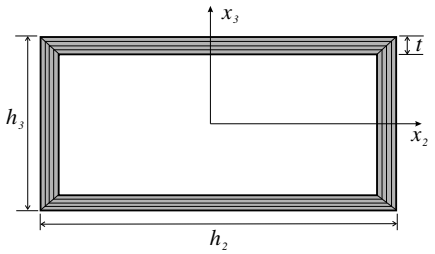

Fig. 7. Cross-sectional geometry of a composite box beam.

Table 1
Layups for a thin-walled box beam

Layup	Upper wall	Right wall	Lower wall	Left wall
Case 1	$[0]_6$	$[0]_6$	$[0]_6$	$[0]_6$
Case 2 (CUS1)	$[15]_6$	$[-15]_6$	$[-15]_6$	$[15]_6$
Case 3 (CAS1)	$[15]_6$	$[15/-15]_3$	$[15]_6$	$[15/-15]_3$
Case 4 (CAS3)	$[45]_6$	$[45/-45]_3$	$[45]_6$	$[45/-45]_3$

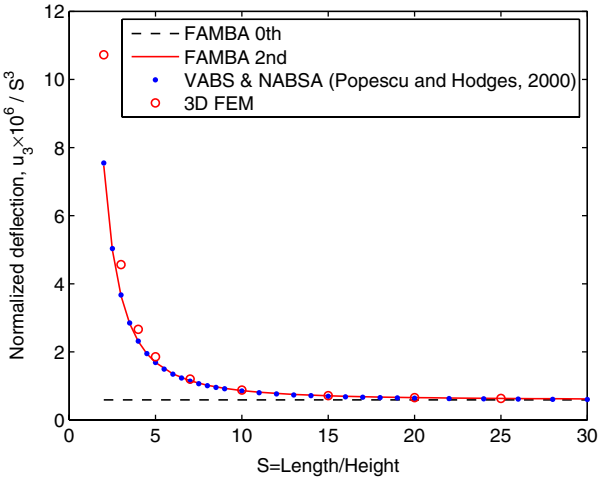

Fig. 8. Tip deflection of an orthotropic box beam with varying length-to-thickness ratio (Case 1).

Popescu and Hodges (2000). NABSA stands for Nonhomogeneous Anisotropic Beam Section Analysis, which is a computer code developed at Georgia Tech by Prof. O. Bauchau based on the work of Giavotto et al. (1983). It is seen that there is no difference among three models in practice, since they are based on the cross-sectional analysis using 2D finite elements so that warping functions can be accurately calculated for this orthotropic box beam.

The first-order cross-sectional deformation mode of an orthotropic box beam is illustrated in Fig. 9, where the in-plane warping and Saint–Venant's torsional warping are clearly seen. Unlike the solid cross-section case presented in Section 6.1, the 3D Poisson's effects are replaced by the combination of local thin-wall beam extension and/or bending modes. Such local deformations are more clearly shown in Fig. 10, where the third-order cross-sectional deformation mode is illustrated. It is worth while to note that even though this specific example does not require such a higher-order in-plane deformation mode, it may be needed for different loading conditions or for the high frequency analysis in vibration problems. This demonstrates that the present FAMBA has capability to provide the in-depth understanding of the behavior of a 3D box beam.

6.2.2. Anisotropic box beams

For Cases 2–4, the bending slope and induced twist distributions along the axial coordinate are presented in Figs. 11–13, where a vertical shear force is applied. There are extension–twist and bending–shear couplings in the CUS configuration, whereas bending–torsion and extension–shear couplings in the CAS configuration. The present results are compared to those obtained by VABS (Yu et al., 2002), NABSA, Jung et al. (2002) and Kim and White (1997) as well as experimental results obtained by Chandra et al. (1990). The results of VABS, NABSA and Jung et al. (2002) presented herein are reproduced by taking their stiffness models from references and applying them to a typical Timoshenko beam model.

In Fig. 11, it can be seen that the present second-order solution is almost same as the zeroth-order solution. This implies that a shear deformation is not significant for this 30 in.-long beam. It is, therefore, hard to distinguish the present FAMBA-0th and -2nd results from 3D FEM results, while those obtained by VABS,

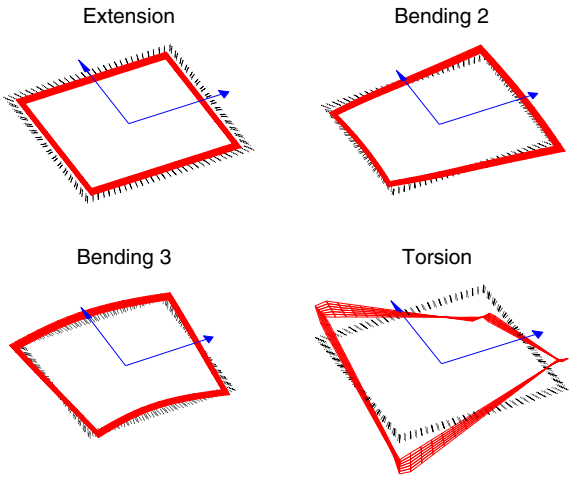

Fig. 9. The first-order cross-sectional deformation mode of an orthotropic box beam, $\Gamma_e^{(1)}$, (Case 1).

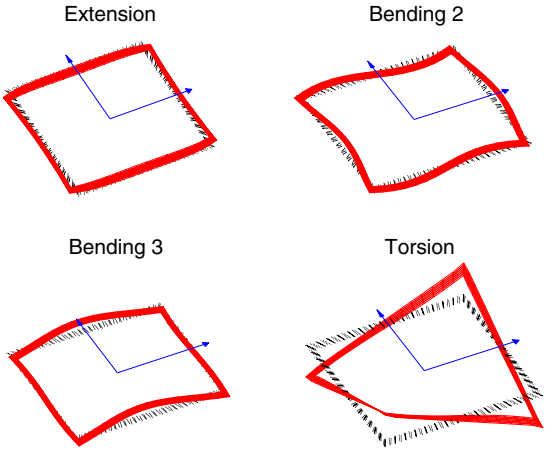

Fig. 10. The third-order cross-sectional deformation mode of an orthotropic box beam, $\Gamma_e^{(3)}$, (Case 1).

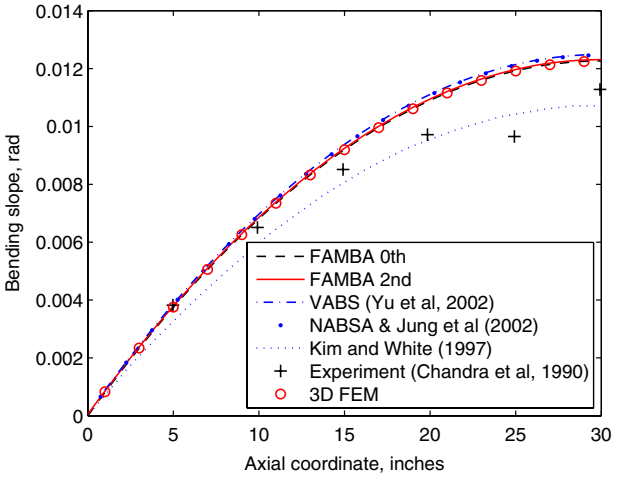

Fig. 11. Bending slope of a CUS1 beam under a vertical shear force (Case 2).

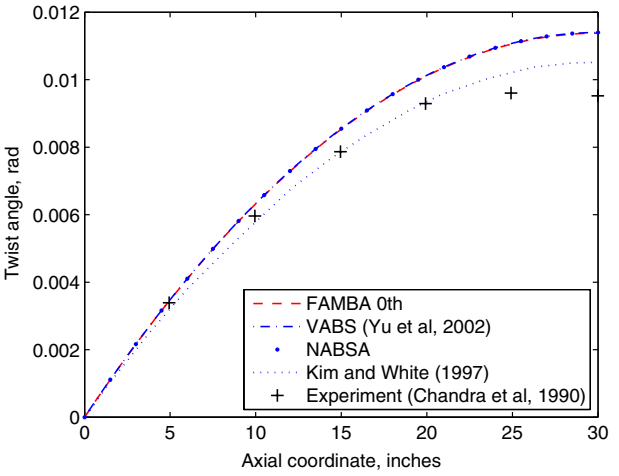

Fig. 12. Induced twist angle of a CAS1 beam under a vertical shear force (Case 3).

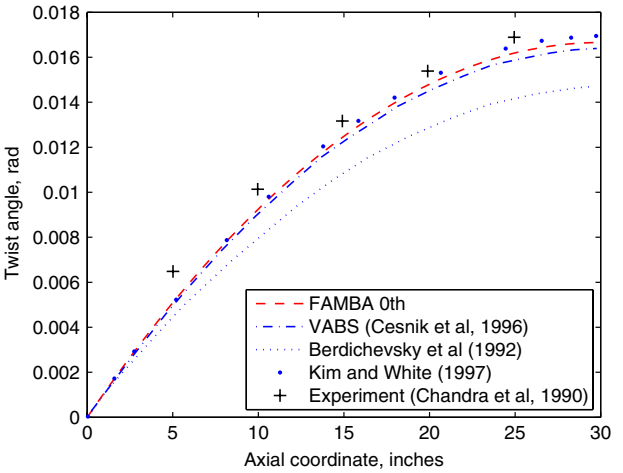

Fig. 13. Induced twist angle of a CAS3 beam under a vertical shear force (Case 4).

NABSA and Jung et al. (2002) slightly deviate from 3D FEM ones. For CAS1 and CAS3 configurations, induced twist distributions due to a vertical shear force are presented in Figs. 12 and 13, respectively. It is of interest to see that the results obtained by Kim and White (1997) and Berdichevsky et al. (1992) are different from the others such as FAMBA, VABS and NABSA, even though Kim and White (1997) have considered the 3D elastic effects and thickness warping and Berdichevsky et al. (1992) have used the variational-asymptotic method without considering thickness effect. This indicates that both local thin-wall deformations (not Poisson's effects in the 3D sense) and thickness effects are important even for the classical behavior of a box beam.

It is not good enough to compare the bending slope and twist angle distributions along the axial coordinate, since all the approaches yield similar results due to the fact that composite box beams considered herein are slender. In order to compare their asymptotic behavior and/or their accuracy of Rankine–Timoshenko-like corrections, normalized transverse deflections against the slenderness ratio are plotted in Figs. 14, 16, 18 and 19. As discussed in Popescu and Hodges (2000) and Yu et al. (2002), the 6×6 stiffness matrix of VABS is different from that of NABSA for the CUS1 configuration (Case 2), whereas that from Jung et al. (2002) is well correlated with NABSA. This case under a horizontal shear force is shown in Fig. 14. It is seen that FAMBA-2nd among others shows the best result as compared to 3D FEM, whereas NABSA, Jung et al. (2002) and

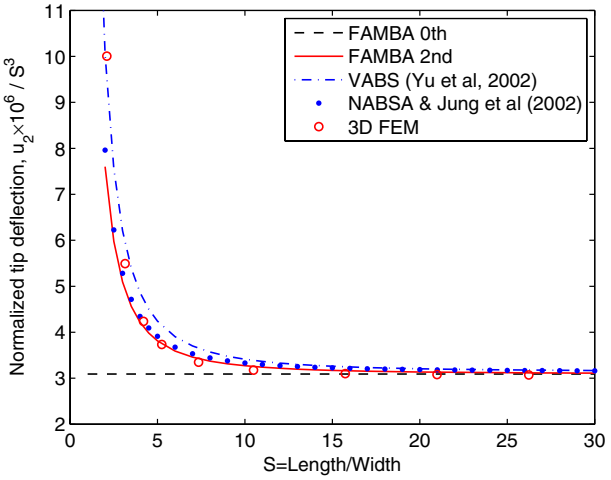

Fig. 14. Tip deflection of a CUS1 beam under a horizontal shear force vs. length-to-width ratio (Case 2).

VABS deviate from 3D FEM even for $S \geqslant 20$ where 3D FEM converges to a classical solution. For 5 in.-long CUS1 beam, the bending slope along the axial coordinate is plotted in Fig. 15. It can be seen that the interior solution is valid approximately 1.5–4 in. from a clamped end. As long as the interior solution is concerned, the present FAMBA-2nd shows an excellent agreement with 3D FEM, whereas VABS deviates from 3D FEM as much as FAMBA-0th (or a classical theory) does.

Induced vertical deflections of a CUS1 beam due to a horizontal shear force is presented in Fig. 16, where deflections are measured from the beam mid-span at which the maximum occurs. It is of interest to see that Rankine–Timoshenko corrections to induced deflections are achieved by not the second-order solution but the first-order one. Unlike the preceding examples such as a sandwich beam and an orthotropic box beam, $\mathcal{A}^{(2)}$ is not zero due to the presence of bending–shear couplings. As expected, induced deflections decay slowly as compared to a direct shear deformation effect shown in Fig. 14. One can see that FAMBA-1st is well correlated with 3D FEM as $S \geqslant 5$, whereas the deviation from 3D FEM of the others is more than 50%. In Fig. 17, induced deflections along the axial coordinate are plotted for a 30 in.-long CUS1 beam. It is clearly seen that VABS and NABSA significantly deviate from 3D FEM qualitatively as well as quantitatively, whereas FAMBA-1st is well correlated with 3D FEM. This demonstrates that boundary conditions, Eq. (72), along with the

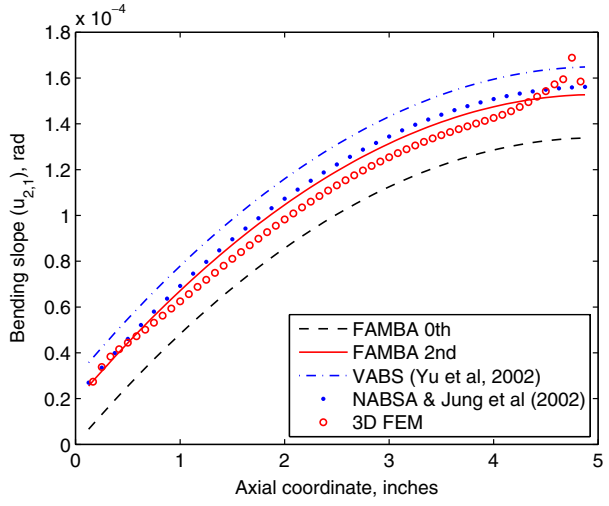

Fig. 15. Bending slope of a CUS1 beam under a horizontal shear force (Case 2), $l = 5$ in.

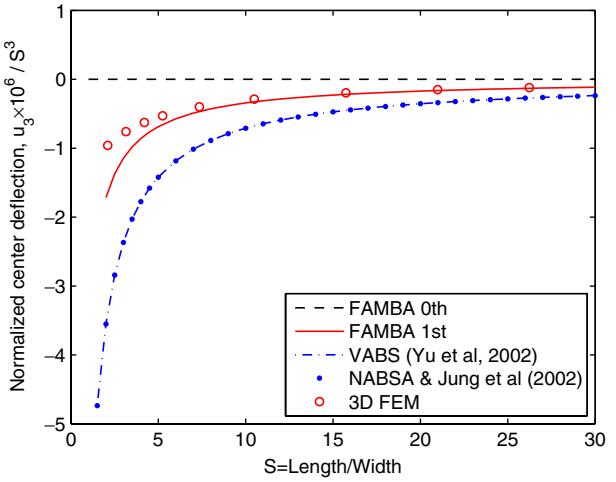

Fig. 16. Induced center deflection of a CUS1 beam under a horizontal shear force vs. length-to-width ratio (Case 2).

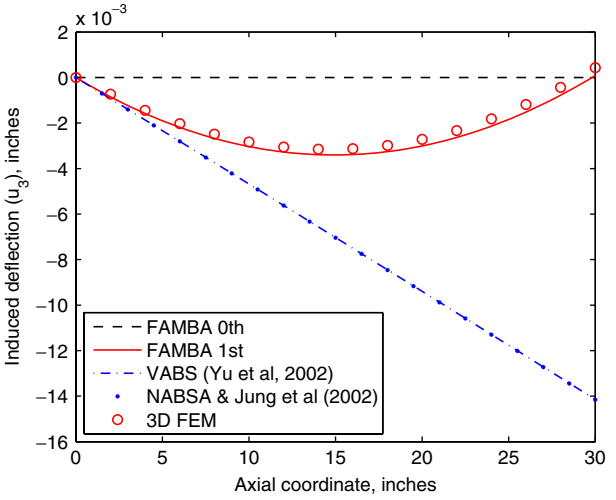

Fig. 17. Induced deflection of a CUS1 beam under a horizontal shear force (Case 2), $l = 30$ in.

fictive volume force, Eq. (63), enable us to find asymptotically correct results up to $O(\epsilon^2)$ for coupled box beams.

For a CAS1 configuration (Case 3), results under a vertical shear force and a tensile force are reported in Figs. 18 and 19, respectively. In Fig. 18, VABS and NABSA are identical, whereas FAMBA-2nd predicts less deflection than they do. Although VABS is based on the similar mathematical foundation, it loses some accuracy during Timoshenko-like energy transformation (Yu et al., 2002). The asymptotic behavior of tension induced deflections is presented in Fig. 19, where three models produce identical results. Although the extension–shear coupling is not presented in a classical Euler–Bernoulli–Navier model, it can be included by considering end effects.

From Figs. 8, 14, 16, 18 and 19, one can conclude that the induced shear deformation effect is more important than the direct one because it affects the qualitative behavior of a beam. These figures actually show that the zeroth-order solution is valid only as the slenderness ratio tends to zero. By contrast, taking into account the higher-order terms of the expansion and using the simplified boundary conditions enable us to enlarge the validity domain of the asymptotic solution.

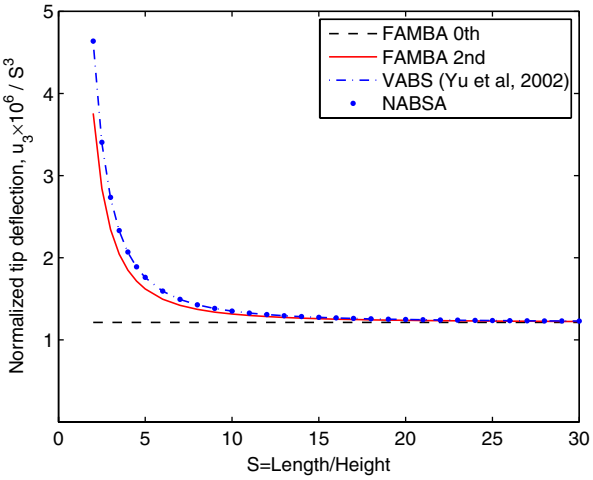

Fig. 18. Tip deflection of a CAS1 beam under a vertical shear force vs. length-to-height ratio (Case 3).

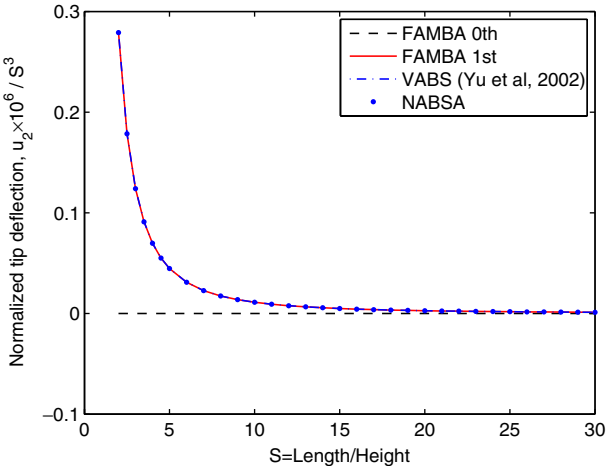

Fig. 19. Tip deflection of a CAS1 beam under a tensile force vs. length-to-height ratio (Case 3).

6.3. An orthotropic D-beam

In order to investigate the accuracy of the present approach for the composite beam of asymmetric cross-sections, an orthotropic D-beam, which is a typical load-carrying structure for helicopter rotor blades, is considered in this subsection. The D-beam dimension and loading conditions are shown in Fig. 20, where the induced torsional load due to asymmetric geometry is presented because the origin of x_2 and x_3 coordinates is located at the centroid of a beam (not the shear center). There are extension–bending and shear–torsion couplings in this D cross-section due to the geometric asymmetry. The ply material properties are the same as those used in Section 6.2. The fiber is aligned parallel to the x_1 coordinate.

The results under a vertical shear force are shown in Fig. 21, where the bending deflection and the twist angle along the axial coordinate are illustrated for 5 in. and 30 in. orthotropic D-beams, respectively. In the 5 in. beam case, the boundary layer (i.e., distortion) for twist angles strongly develops at the free end of a beam due to the localized point loads and asymmetric geometry. For this reason, the twist angles are plotted for the 30 in. beam. The 3D FEM results are obtained using 5400 solid elements. One can see that the present FAMBA works well for the beam of an asymmetric cross-section. It should be noticed here that the non-zero torsion response is appeared at the first-order beam solution. Even though the torsional load is

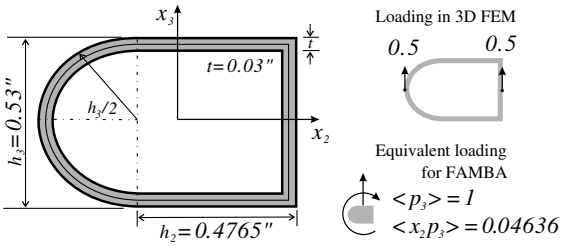

Fig. 20. Geometry of a composite D-beam and loading conditions.

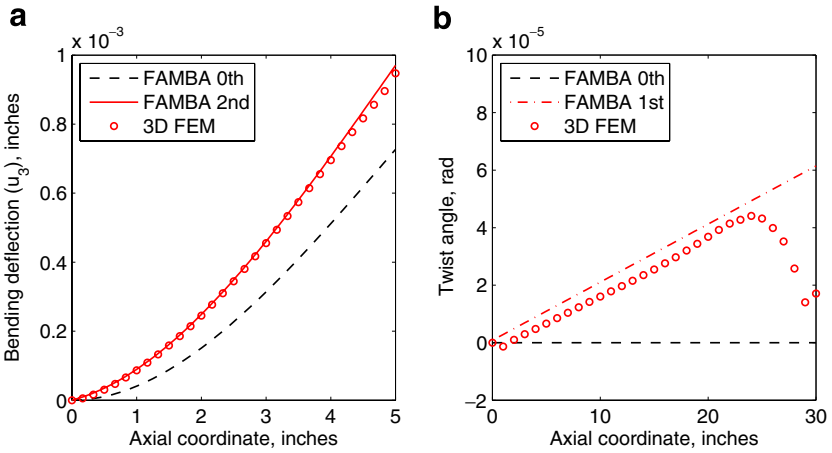

Fig. 21. An orthotropic D-beam under a vertical unit tip load: (a) bending deflection ($l = 5$ in.) and (b) twist angle ($l = 30$ in.).

prescribed at the free end of a beam, it appears at the second beam equations, as shown in Eq. (60). In addition, there is a shear (u_3)–torsion (ϕ) coupling (i.e., $\mathcal{A}^{(2)} \neq 0$), and therefore, the twist angle shown in Fig. 21(b) is affected by both the applied torsion and the shear induced torsion. In fact, each of these torsion causes the large twist angles, $O(10^{-4})$, to the opposite direction, so that it becomes the small twist angle, $O(10^{-5})$.

7. Concluding remarks

A finite element realization of the formal asymptotic method for anisotropic beams having arbitrary cross-sections has been presented in this paper. From the 3D equilibrium equations, a set of 2D microscopic equations and 1D macroscopic equilibrium equations are systematically derived via the formal asymptotic method. Both microscopic and macroscopic equations are completely realized with the finite element method by applying the virtual work concept.

One of difficulties in the formal asymptotic method is to find the asymptotically correct boundary conditions especially for a clamped end. In order to circumvent it, the generalized orthogonality conditions of asymptotic displacements to six fundamental solutions are introduced as constraints, which yields six kinematic boundary conditions at kth order beam problems. The boundary conditions obtained herein are applied to cantilevered composite beams with solid and thin-walled cross-sections. The results are compared to those reported in literature as well as 3D FEM. It is demonstrated that the present FAMBA has capability to provide in-depth understanding as well as accurate predictions of such beams.

We arrive at the same conclusion made in Gregory and Wan (1984), Duva and Simmonds (1991), Fan and Widera (1992) and Buannic and Cartraud (2000, 2001b) saying that *considering end effects makes the use of a refined beam theory unnecessary*. In addition to this, as stated in Duva and Simmonds (1992), we may conclude that *it seems much simpler to abandon Rankine–Timoshenko theory and instead use the iteration scheme outlined*

here to improve elementary theory. Because one may find a correct shear factor only after considering end effects, and the computational effort of solving beam equations is much less than even the cross-sectional analysis.

References

Balch, C.D., Steele, C.R., 1987. Asymptotic solutions for warping and distorsion of thin-walled box beams. Journal of Applied Mechanics 54 (1), 165–173.

Berdichevsky, V.L., 1981. On the energy of an elastic rod. Journal of Applied Mathematics and Mechanics (PMM) 45 (4), 518–529.

Berdichevsky, V.L., Armanios, E.A., Badir, A.M., 1992. Theory of anisotropic thin-walled closed-section beams. Composites Engineering 2, 411–432.

Buannic, N., Cartraud, P., 2000. Higher-order asymptotic model for a heterogeneous beam, including corrections due to end effects. In: 41st AIAA/ASME/ASCE/AHS/ASC Structures, Structural Dynamics, and Material Conference and Exibit. AIAA-2000-1495, Atlanta, GA, USA.

Buannic, N., Cartraud, P., 2001a. Higher-order effective modeling of periodic heterogeneous beams. I. Asymptotic expansion method. International Journal of Solids and Structures 38, 7139–7161.

Buannic, N., Cartraud, P., 2001b. Higher-order effective modeling of periodic heterogeneous beams. II. Derivation of the proper boundary conditions for the interior asymptotic solution. International Journal of Solids and Structures 38, 7168–7180.

Cesnik, C.E.S., Hodges, D.H., 1997. VABS: a new concept for composite rotor blade cross-sectional modeling. Journal of the American Helicopter Society 42 (1), 27–38.

Cesnik, C.E.S., Sutyrin, V.G., Hodges, D.H., 1996. Refined theory of composite beams: the role of short-wavelength extrapolation. International Journal of Solids and Structures 33 (10), 1387–1408.

Chandra, R., Stemple, A.D., Chopra, I., 1990. Thin-walled composite beams under bending, torsional, and extensional loads. Journal of Aircraft 27 (7), 619–626.

Cimetiere, D., Geymonat, G., LeDret, H., Raoult, A., Tutek, Z., 1988. Asymptotic theory and analysis for displacements and stress distribution in nonlinear elastic straight slender rods. Journal of Elasticity 19, 111–161.

Duva, J.M., Simmonds, J.G., 1991. The usefulness of elementary theory for the linear vibrations of layered, orthotropic elastic beams and corrections due to two-dimensional end effects. Journal of Applied Mechanics 58, 175–180.

Duva, J.M., Simmonds, J.G., 1992. The influence of two-dimensional end effects on the natural frequencies of cantilevered beams weak in shear. Journal of Applied Mechanics 59, 230–232.

Fan, H., Widera, G.E.O., 1992. On the proper boundary conditions for a beam. Journal of Applied Mechanics 59, 915–922.

Fan, H., Widera, G.E.O., 1994. On the use of variational principles to derive beam boundary conditions. Journal of Applied Mechanics 61, 470–471.

Giavotto, V., Borri, M., Mantegazza, P., Ghiringhelli, G., Carmashi, V., Maffioli, G.C., Massi, F., 1983. Anisotropic beam theory and applications. Computers and Structures 16, 403–413.

Gregory, R.D., Wan, F.Y.M., 1984. Decaying states of plane strain in a semi-infinite strip and boundary conditions for plate theory. Journal of Elasticity 14, 27–64.

Hodges, D.H., 1990. A review of composite rotor blade modeling. AIAA Journal 28, 561–565.

Horgan, C.O., Simmonds, J.G., 1991. Asymptotic analysis of an end-loaded transversely isotropic, elastic, semi-infinite strip weak in shear. International Journal of Solids and Structures 27, 1895–1914.

Irago, H., Viãno, J., 2002. Saint–Venant's principle in the asymptotic analysis of elastic rods with one end fixed. Journal of Elasticity 66, 21–46.

Jung, S.N., Nagaraj, V.T., Chopra, I., 1999. Assessment of composite rotor blade modeling techniques. Journal of the American Helicopter Society 44, 188–205.

Jung, S.N., Nagaraj, V.T., Chopra, I., 2002. Refined structural model for thin- and thick-walled composite rotor blades. AIAA Journal 40 (1), 105–116.

Kim, C., White, S.R., 1997. Thick walled composite beam theory including 3-D elastic effects and torsional warping. International Journal of Solids and Structures 34 (31–32), 4237–4259.

Kolpakov, A.G., 1991. Calculation of the characteristics of thin elastic rods with a periodic structure. Journal of Applied Mathematics and Mechanics (PMM) 55 (3), 358–365.

Peters, M., Hackl, K., 2005. Numerical aspects of the eXtended finite element method. Proceedings in Applied Mathematics and Mechanics (PAMM) 5, 355–356.

Popescu, B., Hodges, D.H., 2000. On asymptotically correct Timoshenko-like anisotropic beam theory. International Journal of Solids and Structures 37, 535–558.

Savoia, M., Tullini, N., 1996. Beam theory for strongly orthotropic materials. International Journal of Solids and Structures 33 (17), 2459–2484.

Simeon, B., 2006. On Lagrange multipliers in flexible multibody dynamics. Computer Methods in Applied Mechanics and Engineering 195, 6993–7005.

Taylor, R.L., Beresford, P.J., Wilson, E.L., 1976. A non-conforming element for stress analysis. International Journal for Numerical Methods in Engineering 10, 1211–1219.

Trabucho, L., Viãno, J.M., 1996. Mathematical modelling of rods. In: Ciarlet, P.G., Lions, J.L. (Eds.). Handbook of Numerical Analysis, vol. 4. North-Holland, Amsterdam, pp. 487–969.

Volovoi, V.V., Hodges, D.H., Cesnik, C.E.S., Popescu, B., 2001. Assessment of beam modeling methods of rotor blade applications. Mathematical and Computer Modeling 33, 1099–1112.

Yeo, S.T., Lee, B.C., 1997. New stress assumption for hybrid stress elements and refined four-noded plane and eight-noded brick elements. International Journal for Numerical Methods in Engineering 40, 2933–2952.

Yu, W., Hodges, D.H., Volovoi, V.V., Cesnik, C.E.S., 2002. On Timoshenko-like modeling of initially curved and twisted composite beams. International Journal of Solids and Structures 39, 5101–5121.

Yu, W., Hodges, D.H., Volovoi, V.V., Fuchs, E.D., 2005. A generalized Vlasov theory for composite beams. Thin-Walled Structures 43, 1493–1511.